Drug Design, Development and Therapy

Dovepress
open access to scientific and medical research

Open Access Full Text Article

ORIGINAL RESEARCH

Astragaloside IV Alleviates Renal Tubular Epithelial-Mesenchymal Transition via CX3CL1-RAF/MEK/ERK Signaling Pathway in Diabetic Kidney Disease

Yonghui Hu[1,2,*], Wangna Tang[1,2,*], Wenjie Liu[1,2], Zhibo Hu[1,2], Congqing Pan[1,2]

[1]NHC Key Laboratory of Hormones and Development, Tianjin Key Laboratory of Metabolic Diseases, Chu Hsien-I Memorial Hospital & Tianjin Institute of Endocrinology, Tianjin Medical University, Tianjin, People's Republic of China; [2]Tianjin Key Laboratory of Metabolic Diseases, Tianjin Medical University, Tianjin, 300134, People's Republic of China

*These authors contributed equally to this work

Correspondence: Congqing Pan, NHC Key Laboratory of Hormones and Development, Tianjin Key Laboratory of Metabolic Diseases, Chu Hsien-I Memorial Hospital & Tianjin Institute of Endocrinology, Tianjin Medical University, Tianjin, People's Republic of China, Email profpancq@163.com

Background: Epithelial–mesenchymal transition (EMT) plays an important role in interstitial matrix deposition and renal fibrosis in diabetic kidney disease (DKD). It has been verified that Astragaloside IV (AS-IV) is beneficial for ameliorating DKD. However, the underlying mechanisms of AS-IV on regulating EMT in DKD are yet to be established. Accumulated evidence has suggested that C-X3-C motif ligand 1 (CX3CL1) plays a significant role in the progression of EMT.

Purpose: We aimed to investigate whether AS-IV could alleviate EMT by regulating CX3CL1 in DKD and reveal its underlying mechanisms.

Methods: For the in vivo study, mice were divided into the following five groups (n=10): db/m+vehicle, db/db+vehicle, db/db+AS-IV-L (10mg/kg/d), db/db+AS-IV-M (20mg/kg/d), db/db+AS-IV-H (40mg/kg/d). After 12 weeks of treatment, the renal injuries were assessed based on the related parameters of urine, blood and histopathological examination. Immunohistochemistry and Western blotting were used to detect relative proteins levels. Then in HK-2 cells, the molecular mechanism of AS-IV attenuating the EMT in mice with DKD through the CX3CL1-RAF/MEK/ERK pathway was studied.

Results: In the present study, we found that AS-IV reduced urinary protein levels and improved renal pathological damage in DKD mice. Moreover, AS-IV ameliorated the renal tubular EMT induced by hyperglycemia or high glucose (HG), and decreased the expression of CX3CL1 and inhibited the activation of the RAF/MEK/ERK pathway in vivo and in vitro. In HK-2 cells, down-regulation of CX3CL1 suppressed the stimulation of the RAF/MEK/ERK pathway and EMT induced by HG. However, CX3CL1 overexpression eliminated the benefits of AS-IV on the RAF/MEK/ERK pathway and EMT.

Conclusion: In summary, we indicated that AS-IV alleviates renal tubular EMT through the CX3CL1-RAF/MEK/ERK signaling pathway, indicating that CX3CL1 could be a potential therapeutic target of AS-IV in DKD.

Keywords: Astragaloside IV, epithelial–mesenchymal transition, CX3CL1, diabetic kidney disease, renal fibrosis

Introduction

Diabetic kidney disease (DKD) is still the most common microvascular complication of diabetes and the primary cause resulting in end-stage renal disease (ESRD) in the world. According to epidemiological research worldwide, 30–50% of ESRD is caused by DKD approximately.[1] It is reported that DKD has become the leading cause of ESRD in middle-aged and elderly people in China.[2] To delay the progression of DKD, trials with early or with dual renin–angiotensin–aldosterone system (RAAS) blockade, endothelin receptor antagonists, and the antioxidant bardoxolone have been carried out in the past decades, but unfortunately, none has yielded satisfactory results.[3] Therefore, it is significant to

Received: 28 January 2022
Accepted: 15 May 2022
Published: 31 May 2022

look for more effective therapeutic targets and interventions to prevent or treat DKD further to decrease the prevalence of ESRD in the future.[4] It has been established that tubulointerstitial fibrosis is an essential pathological injury in the progression of DKD.[5,6] The sustained kidney injury induced by hyperglycemia or oxidative stress results in renal inflammation, the overexpression of profibrotic factors and myofibroblast proliferation, followed by excessive accumulation of extracellular matrix (ECM) components, destruction of the renal vasculature and ultimately renal fibrosis.[7] The gradual transformation of renal tubular cells from an epithelial phenotype to a mesenchymal phenotype is the main pathological feature of renal epithelial–mesenchymal transition (EMT). In this transformation, renal tubular cells lose epithelial characteristics, such as reduction of E-cadherin expression, and acquire mesenchymal characteristics, such as increased expression of vimentin and α-SMA.[8] Recently, EMT of renal tubular cells has been recognized as the most common cause to induce impaired renal function and a crucial pathogenic alteration for the development of tubulointerstitial fibrosis in DKD.[9] Therefore, inhibiting the EMT of renal tubular cells may be an effective intervention to delay DKD progression.

C-X3-C motif ligand 1 (CX3CL1), also known as fractalkine (FKN), has been demonstrated that participate in inflammatory immune responses. And it constitutes the only member of the CX3C chemokine superfamily which is involved in cell adhesion and regulation of cell growth.[10] CX3CL1 represents one of the factors related to tissue injury and the aggregation of immune cells into the area of injury.[11] It has been suggested that higher plasma CX3CL1 levels were associated with traditional cardiovascular risk factors, prevalent cardiovascular disease (CVD), and diabetes mellitus (DM) in adults with chronic kidney disease (CKD).[12] Furthermore, an increasing body of evidence has suggested that CX3CL1 plays a significant role in the disease progression of DKD.[13,14] A previous investigation revealed that CX3CL1 is upregulated in renal tissues of diabetic animals and the glomerular and peritubular capillaries.[15] Kikuchi et al indicated that high glucose levels, AGEs and cytokine activation upregulate the expression of CX3CL1 in the rat glomeruli and lead to the development of DKD.[16] Besides, it has been reported that protein overload leads to upregulation of CX3CL1 in proximal tubular epithelial cells through NF-κB and p38-MAPK-dependent pathways.[17] Recently, Fu et al revealed the existence of a CX3CL1-Wnt/β-catenin-EMT axis that stimulated the EMT alteration in the kidneys of MRL/lpr mice and HK-2 cells.[10] Moreover, a previous study suggested that CX3CL1 promotes EMT and induces the increase of invasiveness and metastasis in hypoxic androgen-independent prostate cancer cells.[18] Accumulated evidence also suggests an important role for the RAF/MEK/ERK signaling pathway in regulating EMT in multiple diseases,[19,20] including DKD.[21] However, whether the RAF/MEK/ERK signaling pathway is involved in CX3CL1-induced EMT in DKD remains unclear.

Natural products are a significant ready-made resource for the discovery and development of new drugs, many of which may have potential benefits against DKD. Astragaloside IV (AS-IV) is a natural saponin abundant in Astragalus mongholicus Bunge and exhibits a wide range of biological activities. A body of studies has illustrated the renal-protective role of AS-IV, including suppressing renal inflammation,[22] inhibiting renal tubulointerstitial fibrosis, and protecting podocytes.[23] Recent studies show that AS-IV ameliorates renal tubulointerstitial fibrosis, which was not only related to inhibition of tubular EMT and fibroblast activation but also associated with an increase in NO production in the kidney.[7] However, whether AS-IV can inhibit the expression of CX3CL1 and further inhibit EMT to alleviate renal fibrosis in vivo and in vitro is still unclear. This study aimed to assess the benefits of AS-IV on the EMT of renal tubular epithelial cells and renal fibrosis in DKD and to elucidate the underlying mechanisms of these effects.

Materials and Methods

Animals and Treatments

In the present study, 8-week-old db/db (C57BLKS/J-leprdb/leprdb) male mice were selected as a model for type 2 diabetes mellitus (T2DM), and heterozygous control db/m mice were utilized as normal control. All animals were purchased from Jiangsu Jicui Yikang biotechnology co. LTD (Nan Jing, China). Mice were raised under specific pathogen-free conditions. The present investigation was approved by the Experimental Animal Ethical Committee of

Tianjin Medical University, and all animal-related procedures complied with the guidelines of the Guide for the Care and Use of Laboratory Animals of the National Institutes of Health and the guidelines of the Animal Welfare Act.

The db/db mice were randomly assigned into four groups (n=10 each group): db/db+ vehicle, db/db+AS-IV-L, db/db +AS-IV-M, db/db+AS-IV-H. The AS-IV-L group, AS-IV-M group and AS-IV-H group were treated with AS-IV (10, 20 and 40mg/kg/day respectively), the db/m normal control group (n=10) and db/db experimental control treated with the same volume vehicle. The AS-IV dissolved in sodium carboxymethylcellulose (CMC; Yuanye, China), was given by daily gastric gavage to three AS-IV treatment groups. The treatment period for all mice was 12 weeks.

At the end of the intervention, individual metabolic cages were used to collect 24-h urine samples of mice during the last three days of the experiment. Then all mice were anesthetized by intraperitoneal injection of sodium pentobarbital and sacrificed. After collecting blood from their retro orbital venous plexus for biochemical analysis, their kidneys were immediately collected for further experiments. One tissue of each mouse was stored in formalin and used for histological analysis, and the other kidney was frozen at −80°C quickly.

CX3CL1 Enzyme-Linked Immunosorbent Assay (ELISA)

The serum concentration of CX3CL1 was detected with an ELISA kit (MM-44874M2, MEIMIAN, China), and the detection was conducted according to the manufacturer's instructions. We added the five-fold diluted serum samples to the ELISA plate which was pre-coated, then the enzyme-labeled antibody was added after incubating for two hours. After the plate was washed five times, the substrate for color development was added, and then a microplate reader (Bio-Rad, USA) at 450 nm was used to detect the absorbance.

Cell Culture and Intervention

We purchased human proximal tubular epithelial (HK-2) cells from American Type Culture Collection (ATCC). The cells were cultured in a DMEM medium (C11885500BT, Gibco, USA) containing 10% fetal bovine serum (10091–148, Gibco, USA), 200 U/mL penicillin, and 200μg/mL streptomycin (C125C5, NCM Biotech, China). The carbon dioxide concentration in the incubator was 5%, and the temperature was kept at 37°C in a humidified atmosphere. The cells were assigned into groups as follows: (1) the normal glucose (NG) group was maintained in DMEM containing 5.5mM glucose, (2) the mannitol (MA) group was cultured in DMEM containing 5.5mM glucose and 27.8mM mannitol, (3) the cells in high glucose (HG) group were cultured in DMEM containing 33.3mM glucose, and (4) the HG+AS-IV group was incubated in DMEM containing 33.3mM glucose with 40μM AS-IV. The four groups were maintained for 48h under different conditions. The concentrations of glucose (33.3mM) were used based on the previous study.[8] And we selected the concentrations of AS-IV (40μM) according to the results of a Cell Counting Kit 8 (CCK8) assay (Figure S1).

Cell Viability in Response to AS-IV

Cells were incubated with different concentrations of AS-IV at 0, 5, 10, 20, 40, 80, 120 and 160μM in a high (33.3mM) glucose medium for 24 h. Each group included four vice-wells. And the cells were cultured in an incubator as above described. Then the reagents including 100μL DMEM medium and 10μL CCK-8 were added to each well, and the operations were carried out in the dark. At a wavelength of 450nm, the microplate reader (Bio-Rad, USA) was used to examine absorbance.

Histological and Immunohistochemical Staining

We cut the 4μm-thick serial sections from paraffin blocks, and the sections were stained with hematoxylin and eosin (H&E) staining kits (G1120, Solarbio, China), Masson's trichrome (Masson) staining kits (G1346, Solarbio, China), periodic acid-silver methenamine (PASM) staining kits (G1790, Solarbio, China), and periodic acid–Schiff (PAS) staining kits (G1360, Solarbio, China). The areas of at least 60 glomerular tuft profiles per sample were measured using the interactive image analysis system Image-Pro Plus 6.0, from which the mean glomerular Area (mGA) was evaluated. The percentage of PAS staining glomerular-positive areas (fractional mesangial Area [fMA]) was estimated at a fixed color threshold by first defining the glomeruli as the area of interest, which was determined by identifying three to five individual pixels in regions of PAS-positive staining. Finally, the mean mesangial Area (mMA) was calculated according to the formula: (fMA×mGA)/100.

Immunohistochemistry was conducted to analyze the expression of renal EMT-related proteins. In addition, considering that CX3CL1 is a chemokine involved in the inflammatory immune response, we also examined the expression of the inflammatory factors of the renal interstitium. The paraffin-embedded kidney sections were deparaffinized using xylene, hydrated with graded ethanol, antigen retrieval was performed at 95°C for 10 minutes, then blocked with 3%H2O2, and incubated overnight at 4°C with the primary antibodies as follows: anti-E-cadherin (1:50, A11492, ABclonal, China), anti-vimentin (1:100, 10366-1-AP, Proteintech, China), and anti-α-SMA (1:50, 55135-1-AP, Proteintech, China), anti-IL-1β (1:50, 16806-1-AP, Proteintech, China), anti-IL-18 (1:50, 10663-1-AP, Proteintech, China). The next day, the sections were incubated with biotinylated goat anti-rabbit IgG secondary antibodies (LK2001, both 1:200, Sungene Biotech, China) for one hour. Chromogen diamino-benzidine (DAB) was used to observe the labeling condition, and the sections were counter-stained with hematoxylin for nuclear staining. Sections were analyzed using the Image-Pro Plus 6.0 image analysis system.

Preparation of Total Protein Lysates from the Renal Tissues

For the preparation of total protein lysates, renal tissues were collected for protein extraction by RIPA lysis buffer (P0013C, Beyotime, China) containing proteinase and phosphatase inhibitors (ST506, Beyotime, China). After grinding for three minutes, kidney homogenate was centrifugated for 15 minutes, and supernatants were collected for protein measurement. Total protein fractions were quantified using the BCA kit (Thermo Fisher, Cat: 34580). Then, after being washed with 95°C water for 10 minutes, it was stored in a −20°C refrigerator for subsequent Western Blotting analysis.

Western Blotting Analysis

RIPA lysis buffer containing PMSF, phosphatase inhibitors, and loading buffer were used to extract cellular and kidney tissues protein. Then we loaded equal amounts of protein samples on SDS-PAGE gels and transferred them onto nitrocellulose (NC) membranes. After blocking in 5% milk for one hour, the membranes were washed with TBST for three times, each for 10 minutes, and then were incubated at 4 °C overnight with primary antibodies, including: anti-E-cadherin (1:1000, A11492, ABclonal, China), anti-vimentin (1:2000, 10366-1-AP, Proteintech, China), and anti-α-SMA (1:1000, 55135-1-AP, Proteintech, China), anti-CX3CL1 (1:1000, A14198, ABclonal, China), anti-c-Raf (1:1000, 9422T, CST, USA), anti-phospho-c-Raf (Ser338) (56A6) (1:1000, 9427T, CST, USA), anti-MEK1/2 (D1A5) (1:1000, 8727T, CST, USA), anti-phospho-MEK1/2 (Ser217/221) (41G9) (1:1000, 9154T, CST, USA), anti-p44/42 MAPK (ERK1/2) (1:1000, 9102S, CST, USA), anti-phospho-p44/42 MAPK (ERK1/2) (Thr202/Tyr204) (1:1000, 9101S, CST, USA). The next day, after washing with TBST, the membranes were incubated with biotinylated goat anti-rabbit IgG secondary antibodies (both 1:4000, Sungene Biotech, China) for one hour. ECL reagents (K-12045-D50, Advansta, USA) were used to observe chemiluminescence signals. ImageJ software was conducted to quantify blots.

Immunofluorescence Staining of HK-2 Cells

We plated HK-2 cells on a 24-wells culture plate for immunofluorescence staining. After a relevant intervention, the cells were fixed with 4% paraformaldehyde for 10 minutes and permeabilized with 0.1%Triton X-100 for 30 minutes subsequently. Then the cells were blocked with 5%BSA for 30 minutes. After washing with PBS three times, each for five minutes, the cells were incubated overnight at 4°C with the following primary antibodies: anti-E-cadherin (1:50, A11492, ABclonal, China), anti-vimentin (1:50, 10366-1-AP, Proteintech, China), and anti-α-SMA (1:50, 55135-1-AP, Proteintech, China). Subsequently, the cells were incubated with the corresponding FITC-conjugated secondary antibody for one hour, and in DAPI for three minutes. The culture plate was maintained in the dark. Finally, we used a fluorescence microscope equipped with a digital camera to capture the image.

RNA Isolation and Quantitative PCR

We utilized TRIzol reagent (Invitrogen, Carlsbad, USA) to extract RNA. And we used a reverse transcription system kit (O11018, TransGen Biotech, China) to transcribe the collected RNA into cDNA. Real-time PCR was conducted using an iQ5 Detection System (Bio-Rad, Hercules, CA, USA. Primers used to amplify genes encoding E-cadherin, vimentin, α-SMA, CX3CL1, and GAPDH for use with the SYBR Green system were purchased from Sangon Biotech (B532955-0005, Sangon,

Table 1 Primers Used for Transcript Quantification by qPCR

Gene[a]	Primer Sequences (5'-3')[b]
Hs E-cadherin F	AGTCACTGACACCAACGATAAT
Hs E-cadherin R	ATCGTTGTTCACTGGATTTGTG
Hs Vimentin F	TGAATGACCGCTTCGCCAACTAC
Hs Vimentin R	CTCCCGCATCTCCTCCTCGTAG
Hs α-SMA F	CATGAAGTGTGACATCGACATC
Hs α-SMA R	TGATCTTGATCTTCATGGTGCT
Hs CX3CL1 F	TATCAACAGAACCAGGCATCAT
Hs CX3CL1 R	GACCACAGACTCGTCCATTC
Hs GAPDH F	CTCCTCCACCTTTGACGCTG
Hs GAPDH R	TCCTCTTGTGCTCTTGCTGG

Abbreviations: [a]Hs, human; [b]F, forward primer; R, reverse primer.

China) and the sequences of these primers are provided in Table 1. Relative mRNA expression levels in each group were evaluated with the $2^{-\Delta\Delta CT}$ method, and GAPDH was considered as the normalization control.

Wound Healing Assay

HK-2 cells were first subjected to various interventions and then seeded into six-well plates at 70–80% confluence. Wounds were created by scratching using sterile pipette tips when the confluence reached almost 100%. The medium was discarded, and cells were washed with PBS twice, followed by the addition of a fresh normal cell culture medium. The wound area was recorded using light microscopy at 0 and 24 h.

Transfection of siRNA and pReceiver-M90-CX3CL1

HK-2 cells were transfected with a CX3CL1-siRNA (A10001, GenePharma, China) using the transfection reagent (IV1216150, Invigentech, China) and pReceiver-M90-CX3CL1 kits (EX-M0653-M90, GeneCopoeia, Guangzhou, China) using Vector: pReceiver-M90-CX3CL following the manufacturer's instruction. The CX3CL1-siRNA sequence was as follows: Forward: 5′-GCAACAUCACGUGCAGCAATT-3′, Reverse: 5′-UUGCUGCACGUGAUUUGCTT-3'. The pReceiver-M90-CX3CL1 sequence was as follows: Forward: 5'-CAGCCTCCGGACTCTAGC-3', Reverse: 5'-CTCTACAAATGTGGTATGGC-3'. The transfected cells were cultured in a serum-free medium overnight and then incubated with a medium containing 33.3 mM glucose or containing 33.3mM glucose and 40μM AS-IV for 48h.

Statistical Analysis

GraphPad Prism 8.0.1 (GraphPad, San Diego, CA, United States) software was used for statistical analysis. The results of the experimental data are reported in the form of mean±standard deviation (x±SD). A one-way analysis of variance was used as the basis to evaluate the significance of the results. $P<0.05$ was regarded to be significant. Each test has been repeated a minimum of three times.

Results

AS-IV Improved Physical and Biochemical Parameters in DKD Mice

To evaluate the renal function of DKD mice and the effects of AS-IV, we examined the serum creatinine (Scr), blood urea nitrogen (BUN), 24h urine microalbumin (24h-UMA) levels and measured kidney index using standard laboratory equipment. The contents of Scr, BUN and kidney index in db/db mice were increased significantly compared with the db/m mice ($P<0.05$). On the contrary, compared with the experimental control group, AS-IV-L, AS-IV-M and AS-IV-H treatment mice demonstrated a significant decrease in Scr and BUN ($P<0.05$, respectively). Furthermore, compared with db/m mice, db/db mice showed a significant increase in 24h-UMA ($P<0.05$). AS-IV treatment for 12 weeks in the three groups also significantly reduced 24h-UMA levels, and the decrease was the most obvious in the AS-IV-M group

Table 2 Physical and Biochemical Parameters of Experimental Mice

	db/m	db/db	AS-IV-L	AS-IV-M	AS-IV-H
FPG (mM)	11.29±0.74	30.97±3.07*	32.13±4.95*	30.69±3.94*	30.52±4.63*
BUN (mM)	8.59±0.78	14.38±1.61*	9.71±1.08#	8.27±1.0#	8.36±1.05#
Scr (uM)	52.07±13.13	87.33±9.64*	68.1±5.63*#	63.89±6.25*#	71.97±5.54*#
ALT (U/L)	45.9±6.55	76.44±7.88*	75.64±19.56*	73.64±11.81*	75.95±12.17*
AST (U/L)	77.15±11.1	121.07±13.25*	115.62±14.89*	106.35±11.73*	107.62±17.56*
TG (mM)	1.6±0.3	2.06±0.13	1.97±0.55	1.66±0.18	1.72±0.78
TC (mM)	2.29±0.48	3.87±0.38*	3.37±0.6*	3.77±0.78*	3.54±0.78*
KW (mg)	373.6±31.9	424.5±31.9*	386.3±33.7	379.8±34.0	399.8±37.6
KW/BW (mg/g)	14.04±0.91	7.35±0.57*	7.78±0.88*	7.17±0.76*	7.71±1.1*
24h UMA (μg/24h)	10.6±1.8	173.1±28.4*	129.9±15.8*#	100.2±16.1*#	134.9±21.1*#

Notes: Data are expressed as the mean ± SD. *P<0.05, #P<0.05, *db/db vs db/m group, #db/db+AS-IV vs db/db group, n=10 per group.
Abbreviations: AS-IV, Astragaloside IV; AS-IV-L, low-dose AS-IV (10mg/kg/day); AS-IV-M, medium-dose AS-IV (20mg/kg/day); AS-IV-H, high-dose AS-IV (40mg/kg/day); ALT, alanine aminotransferase; AST, aspartate aminotransferase; TG, triglyceride; TC, total cholesterol; BUN, blood urea nitrogen; Scr, serum creatinine; FPG, fasting plasma glucose; 24h UTP, 24-hour urinary total protein; KW, kidney weight; KW/BW, kidney weight to body weight ratio.

(P<0.05). However, compared with db/db experimental control, three AS-IV intervention groups did not exhibit a significant decrease in fasting plasma glucose (FPG), triglyceride (TG), total cholesterol (TC), alanine aminotransferase (ALT), aspartate aminotransferase (AST) levels. (Table 2).

AS-IV Alleviated Renal Pathological Injury in DKD Mice

H&E, Masson, PASM and PAS staining of the renal tissues were performed to observe the effect of AS-IV alleviated renal pathological injury in DKD mice histopathologically. The histological observation of the benefits of AS-IV against kidney damage is illustrated in Figure 1. H&E staining results showed that compared with db/m mice, the proximal renal tubular cells were generally swollen, and the renal tubular epithelial cells were vacuolated in db/db mice, while AS-IV treatment significantly improved these pathological changes. Masson trichrome staining was used to obverse collagen deposition in kidney tissues. Compared with db/m mice, db/db mice in the experimental control group showed significant increases in collagen deposition, while it was alleviated in AS-IV-treated db/db mice, and the most obvious effect of AS-IV on renoprotection is at a dosage of 20 mg/kg/d. Moreover, according to the PASM staining, the db/db mice showed notably glomerular hypertrophy and mesangial matrix expansion, compared with db/m mice. However, these

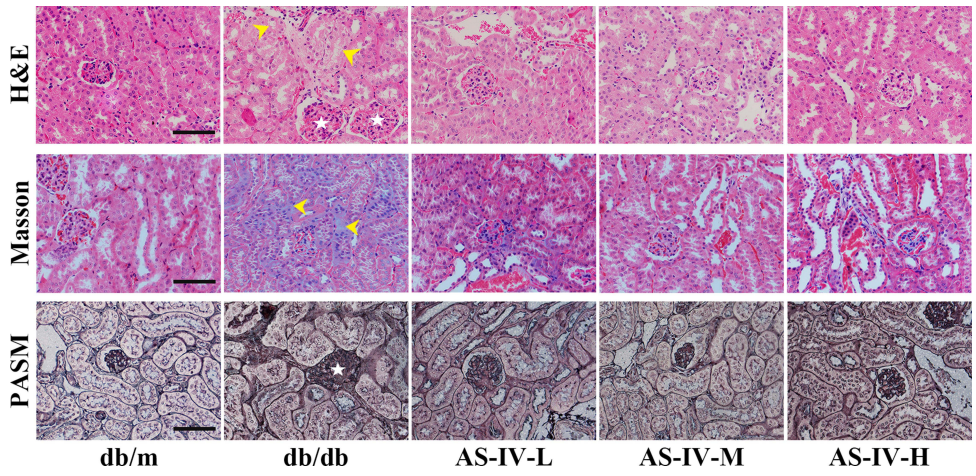

Figure 1 HE staining, Masson staining, and PASM staining for observing changes of the glomerular volume, mesangial matrix expansion, glomerular sclerosis and tubulointerstitial fibrosis in kidneys (stars show glomerular hypertrophy; arrows show swollen renal tubular epithelial cells and tubulointerstitial fibrosis). The scale bar represents 50μm.

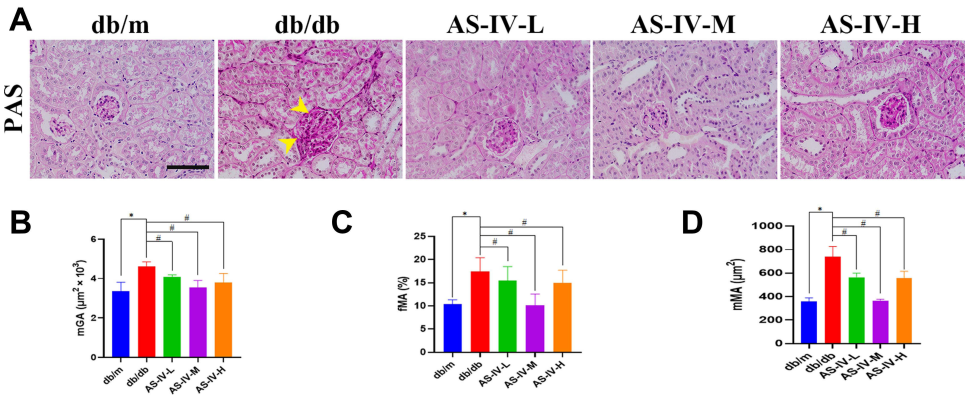

Figure 2 PAS-staining in the kidney (**A**) and quantification of mGA (**B**), fMA (**C**) and mMA (**D**) (arrows show glomerular hypertrophy and mesangial expansion). The scale bar represents 50μm. *P<0.05 vs the db/m group, #P<0.05 vs the db/db group.

histopathological injuries were remarkably attenuated in AS-IV-treated mice. Glomerulopathy was detected in db/db mice, with significantly higher mGA, fMA and mMA, respectively. All these increases were significantly reduced by 12 weeks of AS-IV treatment, respectively (Figures 2A–D). In short, the inhibition of renal fibrosis and the improvement of renal injuries confirmed that AS-IV has a renoprotective effect against the development of DKD.

AS-IV Attenuated Renal EMT and Inhibited the CX3CL1-RAF/MEK/ERK Signaling Pathway in DKD Mice

In this study, we also detected the expression of markers correlate to EMT, including E-cadherin, vimentin and α-SMA expression. The results of immunohistochemistry suggested that the expression levels of vimentin and α-SMA were notably increased, while E-cadherin was decreased in the db/db mice compared with the db/m mice. After AS-IV administration, the expression levels of vimentin and α-SMA were partly suppressed, the E-cadherin expression was partially restored in db/db mice, and the most remarkable effect of AS-IV on renoprotection is at a dosage of 20 mg/kg/d (Figure 3A–F). Besides, compared with the db/m group, the expression IL-1β and IL18 were increased in the db/db group. However, after AS-IV intervention, the expression of IL-1β and IL18 in the renal interstitium was significantly decreased (P<0.05) (Figure 4A–D). To further clarify the role of CX3CL1 in DKD and the anti-EMT

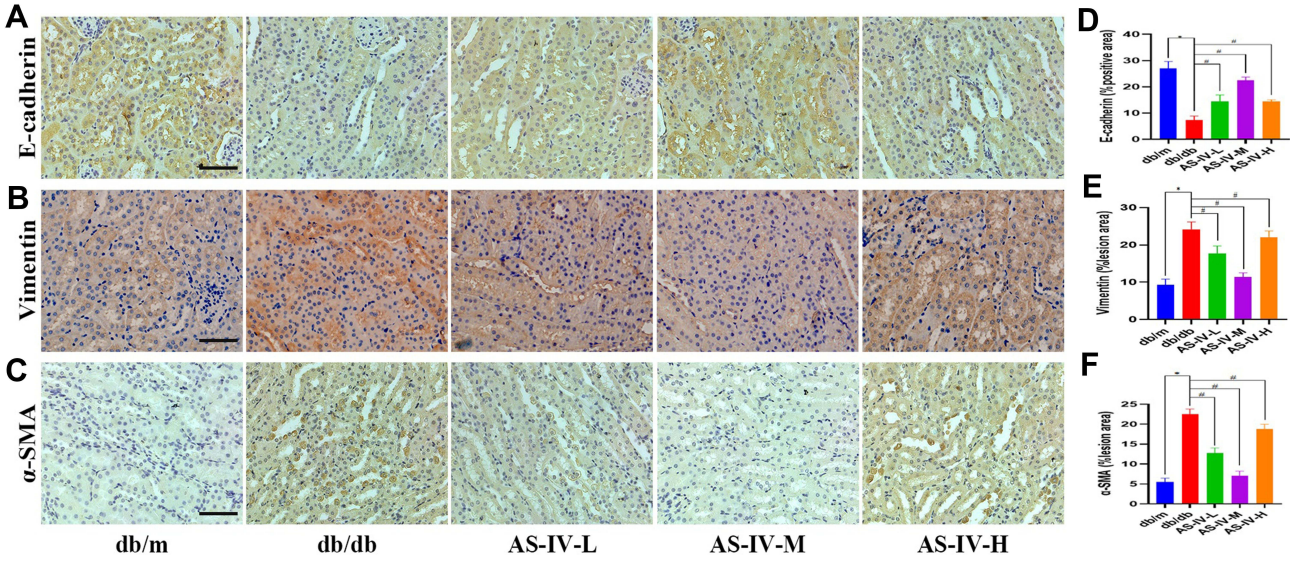

Figure 3 Representative images of E-cadherin (**A**), vimentin (**B**) and α-SMA (**C**) by immunohistochemistry from renal tubules, and quantification of staining (**D**, **E** and **F**, respectively). The scale bar represents 50μm. *P<0.05 vs the db/m group, #P<0.05 vs the db/db group.

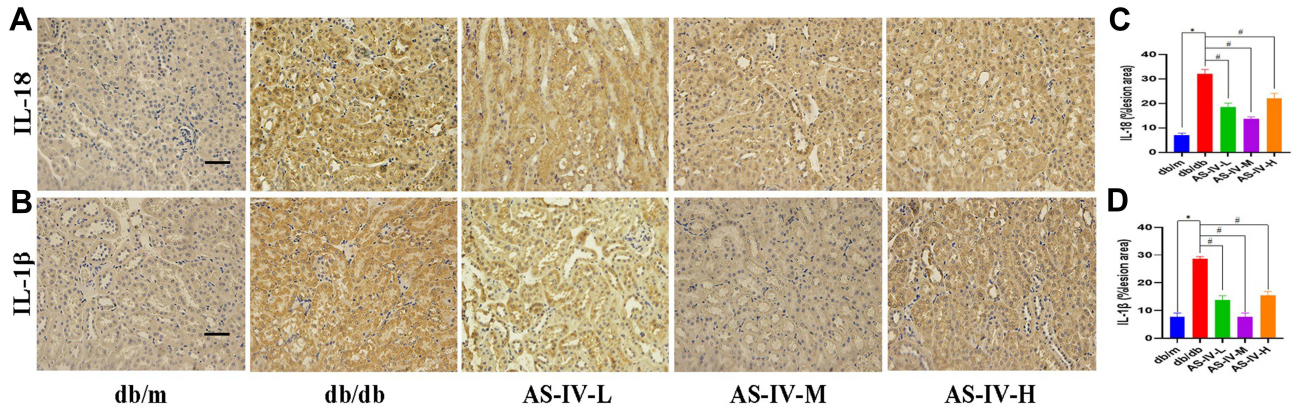

Figure 4 Representative images of IL-18 (**A**) and IL-1β (**B**) by immunohistochemistry from renal tubules, and quantification of staining (**C** and **D**, respectively). The scale bar represents 50μm. *P<0.05 vs the db/m group, #P<0.05 vs the db/db group.

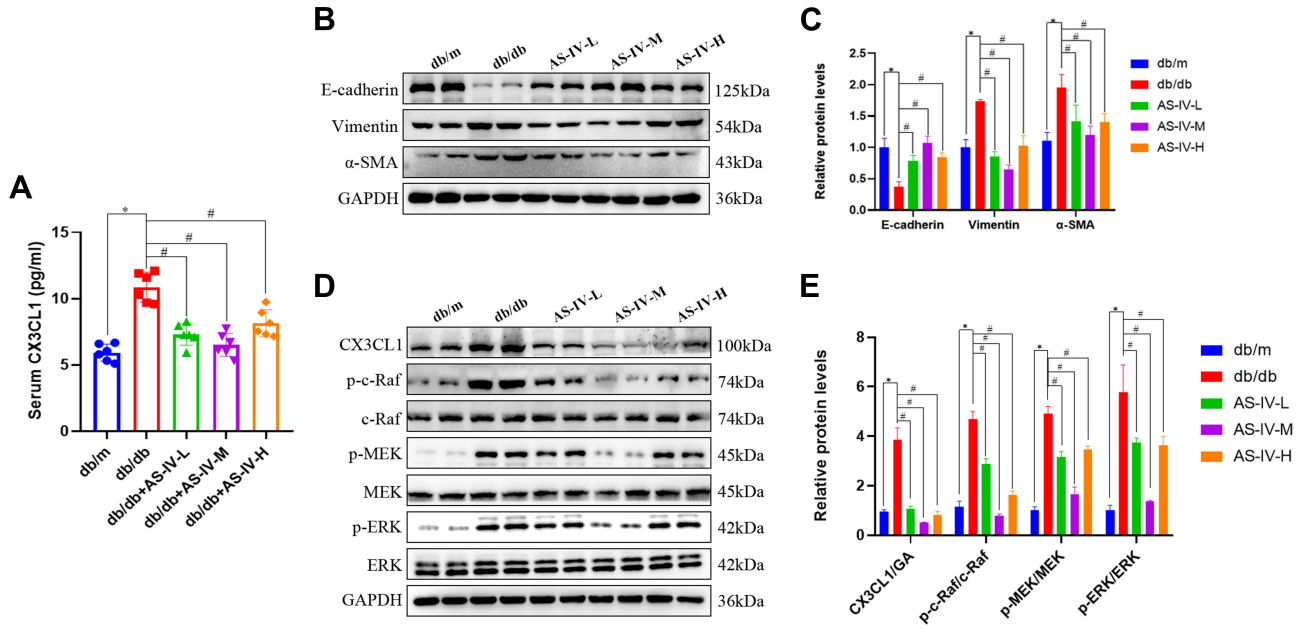

Figure 5 (**A**) The level of CX3CL1 in the serum from db/m or db/db mice (n=6 per group) was detected by ELISA. (**B**) Representative E-cadherin, vimentin and α-SMA bands by Western blot in mice kidneys. (**C**) Densitometric analysis of E-cadherin, vimentin and α-SMA by Western blot (n=5). (**D**) Representative CX3CL1, p-c-Raf, c-Raf, p-MEK, MEK, p-ERK and ERK bands by Western blot in mice kidneys. (**E**) Densitometric analysis of CX3CL1, p-c-Raf/c-Raf, p-MEK/MEK, p-ERK/ERK by Western Blot (n=5). Data are expressed as the mean ± SD. *P<0.05 vs the db/m group, #P<0.05 vs the db/db group.

effects of AS-IV in vivo, the serum levels of CX3CL1 in mice were detected by ELISA kits. The results indicated that the CX3CL1 expression level was significantly increased in db/db mice than that of db/m mice (P<0.05). And after AS-IV intervention, the serum levels of CX3CL1 were significantly decreased in db/db mice (P<0.05), and the decrease was the most obvious in the dose of 20mg/kg/d (Figures 5A). In addition, we also detected the protein levels of vimentin, α-SMA and E-cadherin by Western blotting, which were similar to immunohistochemical results (Figures 5B and C). Additionally, we detected the protein levels of markers in the RAF/MEK/ERK signaling pathway to investigate the underlying molecular mechanisms regarding the anti-EMT benefits of AS-IV. As shown in Figure 5D and E, the ratio of p-c-Raf to t-c-Raf (p-c-Raf/c-Raf), p-MEK1/2 to t-MEK1/2 (p-MEK/MEK), and p-ERK1/2 to t-ERK1/2 (p-ERK/ERK) in db/db mice were increased compared with the db/m group (P<0.05). However, the ratio of p-c-Raf/c-Raf, p-MEK/MEK and p-ERK/ERK protein levels were significantly decreased in AS-IV treated mice

compared with db/db mice without treatment ($P<0.05$). And after AS-IV administration, the CX3CL1 protein levels were also significantly decreased compared with db/db group ($P<0.05$, respectively), and the decrease was the most obvious in the AS-IV-M group.

AS-IV Ameliorated HG-Induced EMT via the CX3CL1-RAF/MEK/ERK Signaling Pathway in vitro

We also explored the anti-EMT benefits of AS-IV in HK-2 cells. As shown in the results of immunofluorescence, it was demonstrated that the vimentin and α-SMA levels were significantly increased and the level of E-cadherin expression was significantly decreased in the HG group. After AS-IV intervention, the EMT of HK-2 cells was suppressed to a great extent (Figure 6A). Subsequently, we conducted qPCR and Western blot analyses, and the results suggested that the AS-IV intervention reduced the mRNA and protein levels of CX3CL1, vimentin and α-SMA and increased the E-cadherin levels compared with the HG group ($P<0.05$, respectively) (Figure 6B–D). In addition, the ratio of p-c-Raf/c-Raf, p-MEK/MEK and p-ERK/ERK were significantly increased in the HG group compared with the NG group, while AS-IV treatment significantly reduced these parameters ($P<0.05$) (Figure 6E and F). To exclude the interference of hyperostosis, the mannitol (MA) group was designed, and there existed no significant difference between

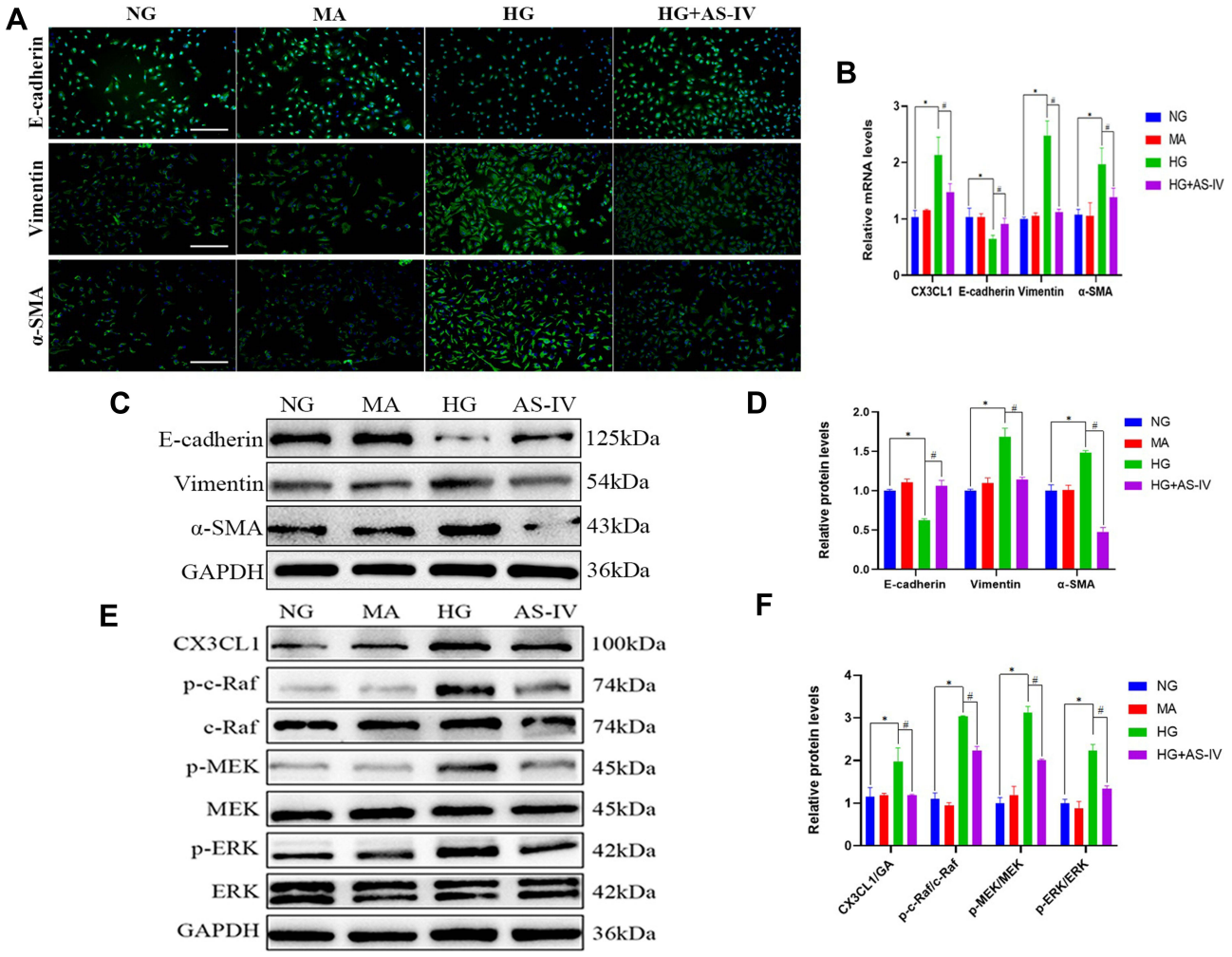

Figure 6 (**A**) Representative images of E-cadherin (green), vimentin (green) and α-SMA (green) by immunofluorescence in HK-2 cells. Blue staining refers to the DAPI-stained nuclei. The scale bar represents 100μm. (**B**) Quantification of CX3CL1, E-cadherin, vimentin and α-SMA gene expression in HK-2 cells (n=4). (**C**) Representative E-cadherin, vimentin and α-SMA bands by Western blot in HK-2 cells. (**D**) Densitometric analysis of E-cadherin, vimentin and α-SMA by Western blot (n=4). (**E**) Representative CX3CL1, p-c-Raf, c-Raf, p-MEK, MEK, p-ERK and ERK bands by Western blot in HK-2 cells. (**F**) Densitometric analysis of CX3CL1, p-c-Raf/c-Raf, p-MEK/MEK, p-ERK/ERK by Western Blot (n=4). Data are expressed as the mean ± SD. *$P<0.05$ vs the NG group, $^{\#}P<0.05$ vs the HG group.

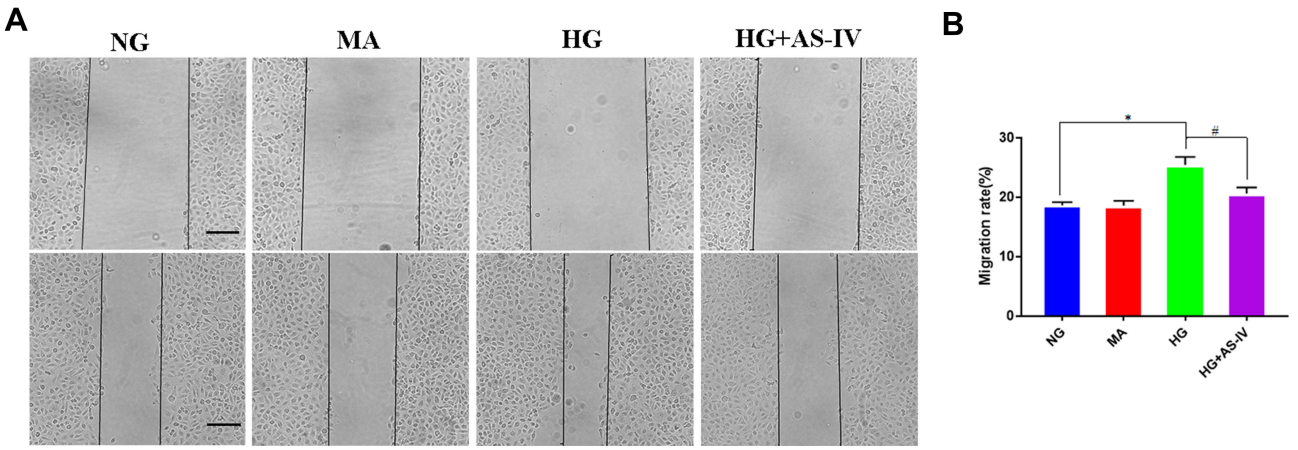

Figure 7 (**A**) Wound healing assay was used to detect cell migration. (**B**) Migration rate (%) of cell migration by wound healing assay. *P<0.05 vs the NG group, #P<0.05 vs the HG group.

the MA group and the NG group. Moreover, as shown by wound healing assays (Figure 7A and B), HG significantly increased HK-2 cells migration, and this progress was partially inhibited after AS-IV intervention (P<0.05). These results further demonstrated that AS-IV ameliorated HG-induced EMT via the CX3CL1 and RAF/MEK/ERK signaling pathway in HK-2 cells.

CX3CL1-siRNA Alleviated HG-Induced EMT and Inhibited the RAF/MEK/ERK Pathway in HK-2 Cells

To further clarify whether CX3CL1 mediated HG-induced EMT via the RAF/MEK/ERK signaling pathway, a CX3CL1 knockout model was constructed in HK-2 cells. After cells were transfected with a CX3CL1-siRNA in HG conditions, the protein levels of vimentin and α-SMA were significantly reduced while E-cadherin level was significantly increased compared with the HG group, which was similar to the effect of AS-IV (P<0.05) (Figure 8A and B). Moreover, the protein level of CX3CL1 and the ratio of p-c-Raf/c-Raf, p-MEK/MEK and p-ERK/ERK were significantly decreased after the abrogation of CX3CL1 expression in HK-2 cells (P<0.05) (Figure 8C and D). These results indicated that the CX3CL1-siRNA had similar benefits as AS-IV, therefore, CX3CL1 may be essential for regulating HG-induced EMT.

C-Raf-Inhibitor Ameliorated HG-Induced EMT in HK-2 Cells

To elucidate the crucial role of the RAF/MEK/ERK signaling pathway in AS-IV-involved in anti-EMT effect, c-Raf inhibitor, Dabrafenib (10μM), was selected to intervene HK-2 cells. And after 48 h the protein levels of the markers related to EMT, CX3CL1 and ratio of p-c-Raf/c-Raf, p-MEK/MEK and p-ERK/ERK were examined. After cells were treated with Dabrafenib in HG conditions, the protein levels of vimentin and α-SMA were also significantly reduced while E-cadherin level was significantly increased compared with the HG group (P<0.05) (Figure 9A and B). The cellular expression of c-Raf was inhibited significantly after the treatment with Dabrafenib. Furthermore, the ratio of p-c-Raf/c-Raf, p-MEK/MEK and p-ERK/ERK was decreased significantly in HK-2 cells, which was similar to the results of AS-IV (P<0.05). However, the protein levels of CX3CL1 were not changed before and after Dabrafenib intervention (Figure 9C and D). Therefore, these data demonstrated that CX3CL1 is upstream of RAF/MEK/ERK signaling pathway.

The Anti-EMT Effects of AS-IV Were Inhibited by pReceiver-M90-CX3CL1

To verify the important role of CX3CL1 in EMT, we overexpressed the CX3CL1 gene by treating HK-2 cells with pReceiver-M90-CX3CL1. After the intervention of pReceiver-M90-CX3CL1, the anti-EMT effects of AS-IV were inhibited by pReceiver-M90-CX3CL1 (Figure 10A and B), and the protein level of CX3CL1 was increased significantly. Furthermore, the ratio of p-c-Raf/c-Raf, p-MEK/MEK and p-ERK/ERK was increased significantly in CX3CL1-overexpressing HK-2 cells (P<0.05). However, the protein levels of CX3CL1 were not changed before and after c-Raf

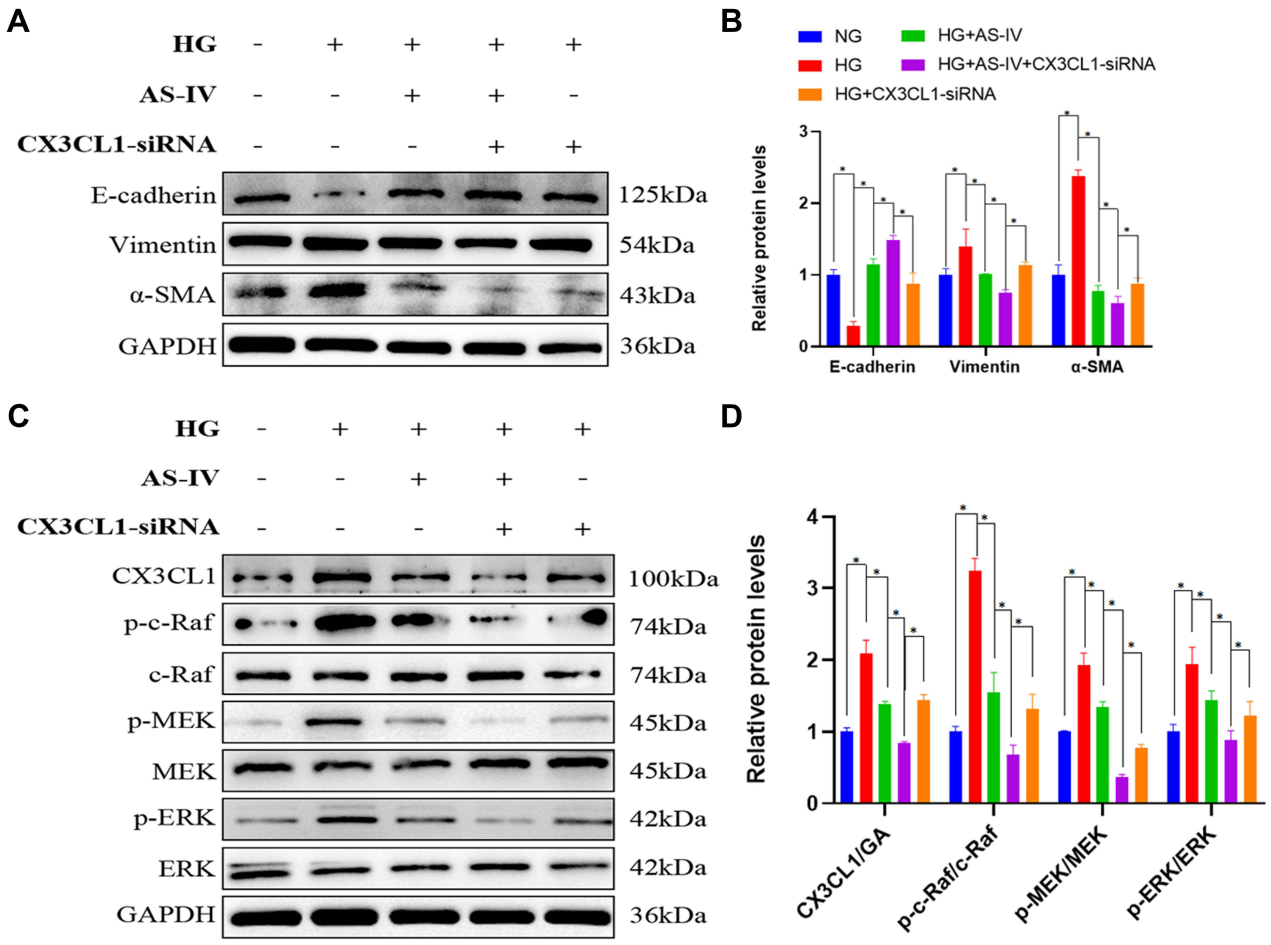

Figure 8 (**A**) Western blot was performed to determine the protein levels of E-cadherin, vimentin and α-SMA in HK-2 cells. (**B**) The expression levels of E-cadherin, vimentin and α-SMA were measured for each group. (n=4). (**C**) Western blot was performed to determine the protein levels of CX3CL1, p-c-Raf, c-Raf, p-MEK, MEK, p-ERK and ERK bands in HK-2 cells. (**D**) The expression levels of CX3CL1, p-c-Raf/c-Raf, p-MEK/MEK, p-ERK/ERK were measured for each group(n=4). Data are expressed as the mean±SD. *P<0.05.

inhibitor treatment (Figure 10C and D). Convincingly, these outcomes also demonstrated that CX3CL1 is upstream of RAF/MEK/ERK signaling pathway.

Discussion

The present in vivo and in vitro studies demonstrate that CX3CL1 aggravated EMT by promoting the RAF/MEK/ERK signaling pathway and that AS-IV ameliorated EMT by inhibiting the expression of CX3CL1 in DKD. AS-IV, a main bioactive component of Astragalus membranaceus (Fisch) Bge (Astragalus), has been widely used to treat DKD clinically in China for hundreds of years.[24,28,29] In this study, AS-IV significantly ameliorated renal function, and 24-h UMA in db/db mice with DKD and effectively alleviated the renal histopathological injuries in db/db mice, which are consistent with previous research.[25,26] Notably, AS-IV had no significant effect on fasting glucose levels in db/db mice, which indicated that AS-IV ameliorated renal tissue damage and proteinuria in a glucose-independent manner. A recent systematic review suggested that AS-IV exerts renal protective effects in animals with DKD through multiple signaling pathways, including relieving oxidative stress, delaying renal fibrosis, anti-apoptosis and anti-inflammatory action.[27] In the present study, AS-IV treatment alleviated renal interstitial inflammation significantly in DKD mice, consistent with previous findings.[28] Feng et al reported that AS-IV ameliorated renal functions and podocyte injury and delayed the development of DKD in db/db mice via anti-NLRP3 inflammasome-mediated inflammation.[29] And a recent study

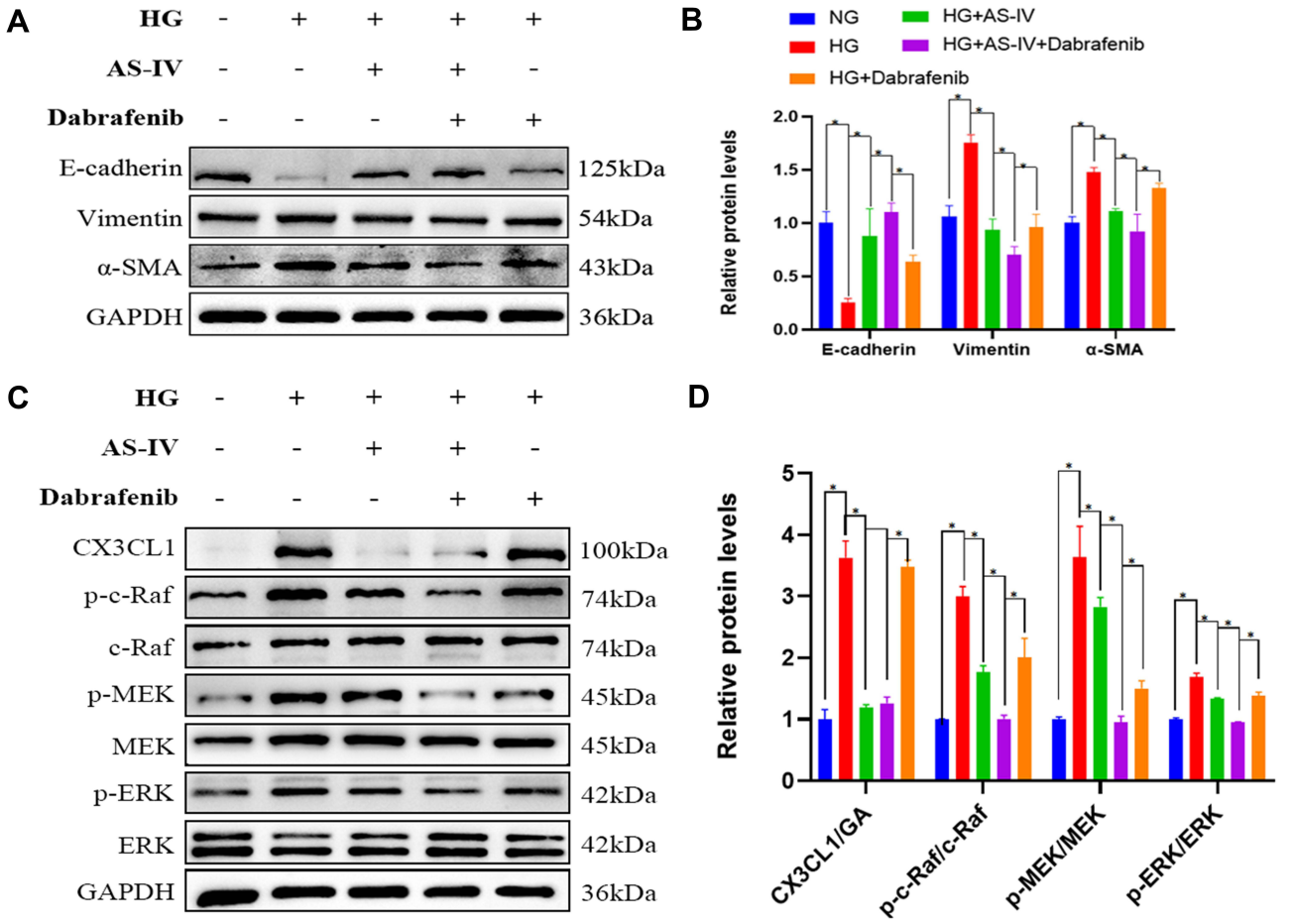

Figure 9 (**A**) Representative E-cadherin, vimentin and α-SMA bands by Western blot in HK-2 cells. (**B**) Densitometric analysis of E-cadherin, vimentin and α-SMA by Western blot (n=4). (**C**) Representative CX3CL1, p-c-Raf, c-Raf, p-MEK1/2, MEK1/2, p-ERK and ERK bands by Western blot in HK-2 cells. (**D**) Densitometric analysis of CX3CL1, p-c-Raf/c-Raf, p-MEK/MEK, p-ERK/ERK by Western blot (n=4). Data are expressed as the mean ± SD. *P<0.05.

showed that AS-IV inhibited palmitate-mediated oxidative stress and fibrosis in human glomerular mesangial cells via downregulation of CD36 expression.[30] Additionally, Wang et al found that AS-IV ameliorated HG-induced EMT of podocytes through autophagy enhancement via the SIRT-NF-κB p65 axis.[31]

It has been confirmed that EMT is crucial in the progression of renal fibrosis in DKD.[32] In this study, we found that EMT was induced by hyperglycemia in DKD mice and HG in HK-2 cells, which was inhibited partially by AS-IV. A previous study indicated that AS-IV suppresses EMT induced by TGF-β1 by inhibiting the PI3K/Akt/NF-κB pathway in gastric cancer cells.[33] Moreover, it has been reported that AS-IV ameliorates EMT induced by HG through inhibition of the TGF-β/Smad signaling cascade in renal proximal tubular epithelial cells.[34] In the present study, we also verified that AS-IV ameliorates renal EMT both in vivo and in vitro. There is accumulating evidence indicating that the RAF/MEK/ERK signaling pathway plays an important role in EMT during DKD.[35,36] It has been demonstrated that the response of ERK/MAPK signaling cascades activation to growth factors or mutant RAS could up-regulate TGF-β-induced EMT.[37] A previous study revealed that the RAF signaling pathway increases the expression of SNAIL1 and/or SNAIL2, thereby promoting cancer-associated EMT manifested as cell motility and invasive behavior upregulation.[38] However, few studies reported whether the RAF/MEK/ERK signaling pathway was involved in the anti-EMT effects of AS-IV in vivo and in vitro. In this study, we found that AS-IV significantly reduced the activation of the RAF/MEK/ERK pathway in DKD mice and HK-2 cells. Convincingly, we indicated that the RAF/MEK/ERK signaling pathway was the potential mechanism of AS-IV mitigating EMT of DKD.

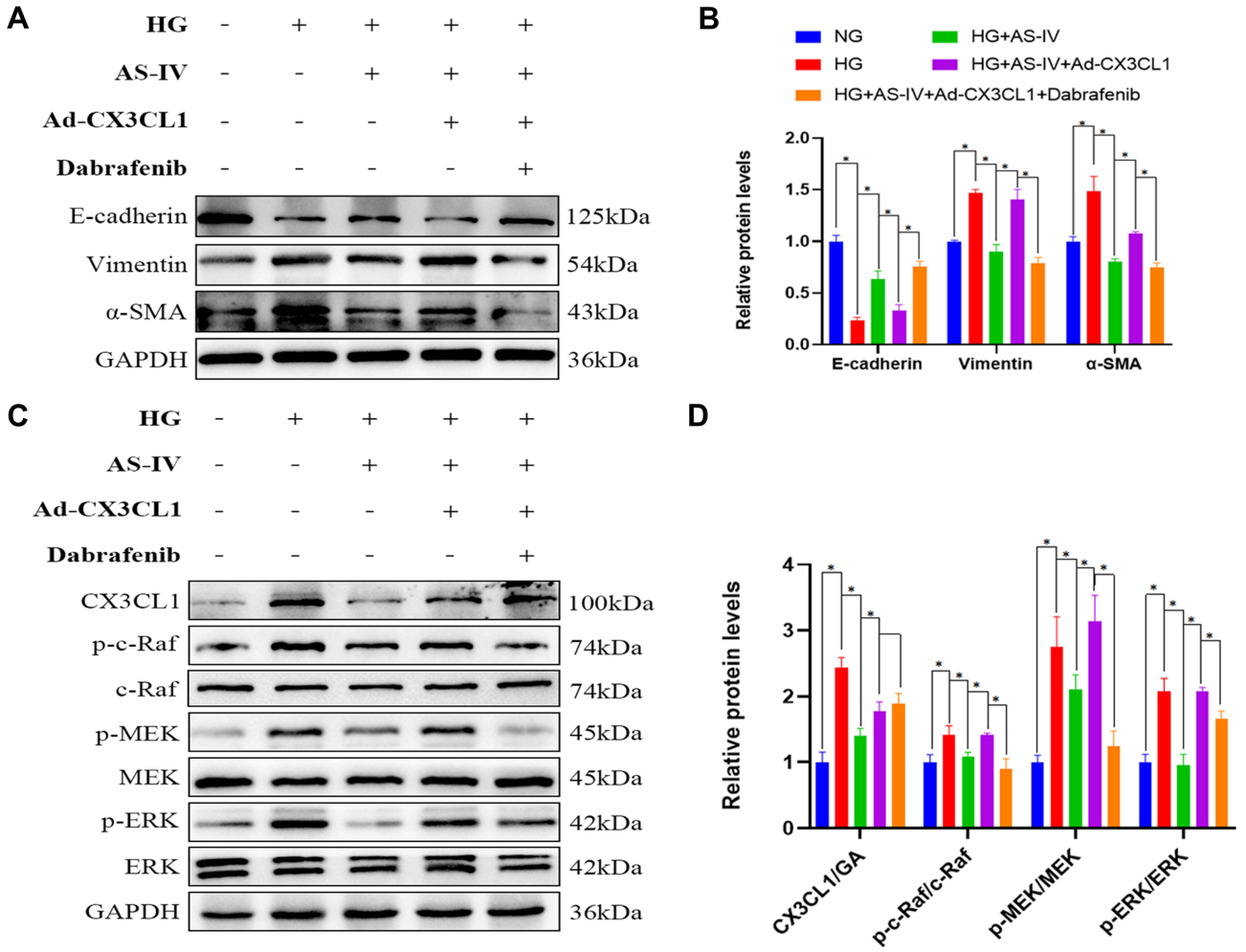

Figure 10 (**A**) Representative E-cadherin, vimentin and α-SMA bands by Western blot in HK-2 cells. (**B**) Densitometric analysis of E-cadherin, vimentin and α-SMA by Western blot (n=4). (**C**) Representative CX3CL1, p-c-Raf, c-Raf, p-MEK, MEK, p-ERK and ERK bands by Western blot in HK-2 cells. (**D**) Densitometric analysis of CX3CL1, p-c-Raf/c-Raf, p-MEK/MEK, p-ERK/ERK by Western blot (n=4). Data are expressed as the mean±SD. *P<0.05.

Increasing evidence elucidates that CX3CL1 is over-expressed in many renal diseases and is regulated by complicated regulatory systems.[39] Several previous studies found that CX3CL1expression is significantly higher in persons with diabetes mellitus than in healthy controls in peripheral blood mononuclear cells and serum.[12,40] It is noteworthy that CX3CL1 is positively correlated with the pathogenesis and progression of DKD.[13] A recent study also revealed that CX3CL1 expression levels were increased in HK-2 cells after lipopolysaccharide stimulation, and with the decrease of CX3CL expression level, renal function of mice improved and kidney injuries alleviated.[10] Additionally, it demonstrated that CX3CL1 was involved in EMT progression through the Wnt/β-catenin pathway, which further accelerated the development of lupus nephritis. However, it remains unclear whether CX3CL1 was involved in the progress of tubular EMT in DKD through RAF/MEK/ERK pathway. Our findings firstly indicated that CX3CL1 knockout protected HK-2 cells from HG-induced RAF/MEK/ERK pathway activation and EMT. In addition, AS-IV treatment could ameliorate EMT by inhibiting the expression of CX3CL1 in vivo and in vitro.

Some scholars have reported that CX3CL1 stimulates MMP-3 generation via the c-RAF, MEK, and ERK signaling pathways.[41] And it has been proposed that CX3CL1 activates the RAF-1/MEK/ERK-dependent signaling pathways, therefore prompting angiogenesis.[42] Therefore, to clarify the involvement of CX3CL1 in this signaling pathway, we confirmed that inhibiting CX3CL1 expression by administration with a CX3CL1-specific siRNA transfection inhibits the activation of RAF/MEK/ERK signaling pathway in HK-2 cells. Moreover, we overexpressed CX3CL1 by transfecting pReceiver-M90-CX3CL1 to investigate the alteration of the activation of the RAF/MEK/ERK signaling pathway. And the results suggested

that the ratio of p-c-Raf/c-Raf, p-MEK/MEK and p-ERK/ERKwas increased significantly in CX3CL1-overexpressing HK-2 cells. Besides, we used Dabrafenib, a c-Raf inhibitor, to investigate the effect of inhibiting this pathway and the expression changes of CX3CL1. The data indicated that the protein levels of CX3CL1 were not changed before and after Dabrafenib intervention, confirming that the CX3CL1 is upstream of RAF/MEK/ERK signaling pathway.

Taken together, our study demonstrated that overexpression of CX3CL1 in HK-2 cells prompts the development of tubular EMT and plays a significant role via a CX3CL1-RAF/MEK/ERK-EMT axis in HK-2 cells. Furthermore, we investigated the role of CX3CL1 in the progression of EMT in DKD mice. Our data suggested that CX3CL1 was involved in EMT development by activating RAF/MEK/ERK signaling, which further increased the probability of EMT leading to DKD. Moreover, we firstly confirmed that AS-IV treatment could inhibit RAF/MEK/ERK pathway by inhibiting the expression of CX3CL1 further ameliorating EMT in DKD. These data suggest the potential of CX3CL1 as a biomarker and therapeutic target in DKD and provide evidence for developing AS-IV as a novel anti-EMT agent against renal fibrosis in DKD.

However, some limitations should be noted in our research. Firstly, although we verified that AS-IV alleviated renal pathological damage and renal tubular EMT, we did not establish any CX3CL1 overexpression or suppression models in vivo. In the future, CX3CL1-treated or gene-knockout animal models are needed to solve this issue. Secondly, we did not evaluate whether over-expressed CX3CL1 is connected with mesangial cells and podocytes, while glomerular fibrosis also existed in DKD. Therefore, more research is warranted to elucidate the above issues.

Conclusions

In conclusion, the present study indicated that AS-IV alleviates renal tubular EMT through the CX3CL1-RAF/MEK/ERK signaling pathway, and CX3CL1 could be a potential therapeutic target of AS-IV in DKD.

Abbreviations

EMT, epithelial–mesenchymal transition; DKD, diabetic kidney disease; AS-IV, Astragaloside IV; Scr, serum creatinine; BUN, blood urea nitrogen; 24h-UTP, 24 h urine total protein; HG, high glucose; ESRD, end-stage-renal disease; RAAS, renin–angiotensin–aldosterone system; ECM, extracellular matrix; CX3CL1, C-X3-C motif ligand 1; FKN, fractalkine; CVD, cardiovascular disease; DM, diabetes mellitus; CKD, chronic kidney disease; H&E, hematoxylin and eosin; PAS, periodic acid–Schiff; PASM, periodic acid-silver methenamine; Masson, Masson's trichrome; mGA, mean glomerular area; fMA, fractional mesangial Area; mMA, mean mesangial Area; FPG, fasting plasma glucose; TG, triglyceride; TC, total cholesterol; ALT, alanine aminotransferase; AST, aspartate aminotransferase; MA, mannitol; NG, normal glucose.

Funding

This work was supported by the National Natural Science Foundation of China (No. 81873304).

Disclosure

The authors report no conflicts of interest in this work.

References

1. Tuttle KR, Bakris GL, Bilous RW, et al. Diabetic kidney disease: a report from an ADA Consensus Conference. *Am J Kidney Dis*. 2014;64(4):510–533. doi:10.1053/j.ajkd.2014.08.001
2. Zhang Y, Jin D, Kang X, et al. Signaling pathways involved in diabetic renal fibrosis. *Front Cell Dev Biol*. 2021;9:696542. doi:10.3389/fcell.2021.696542
3. Perez-Gomez MV, Sanchez-Niño MD, Sanz AB, et al. Horizon 2020 in diabetic kidney disease: the clinical trial pipeline for add-on therapies on top of renin angiotensin system blockade. *J Clin med*. 2015;4(6):1325–1347. doi:10.3390/jcm4061325
4. McCullough KP, Morgenstern H, Saran R, Herman WH, Robinson BM. Projecting ESRD incidence and prevalence in the United States through 2030. *J Am Soc Nephrol*. 2019;30(1):127–135. doi:10.1681/ASN.2018050531
5. Li Y, Hu Q, Li C, et al. PTEN-induced partial epithelial-mesenchymal transition drives diabetic kidney disease. *J Clin Invest*. 2019;129(3):1129–1151. doi:10.1172/JCI121987
6. Zhang Q, Liu X, Sullivan MA, Shi C, Deng B. Protective effect of Yi Shen Pai Du formula against diabetic kidney injury via inhibition of oxidative stress, inflammation, and epithelial-to-mesenchymal transition in db/db mice. *Oxid Med Cell Longev*. 2021;2021:7958021. doi:10.1155/2021/7958021

7. Meng LQ, Tang JW, Wang Y, et al. Astragaloside IV synergizes with ferulic acid to inhibit renal tubulointerstitial fibrosis in rats with obstructive nephropathy. *Br J Pharmacol*. 2011;162(8):1805–1818. doi:10.1111/j.1476-5381.2011.01206.x
8. Xue M, Cheng Y, Han F, et al. Triptolide attenuates renal tubular epithelial-mesenchymal transition via the MiR-188-5p-mediated PI3K/AKT pathway in diabetic kidney disease. *Int J Biol Sci*. 2018;14(11):1545–1557. doi:10.7150/ijbs.24032
9. Xu Z, Jia K, Wang H, et al. METTL14-regulated PI3K/Akt signaling pathway via PTEN affects HDAC5-mediated epithelial-mesenchymal transition of renal tubular cells in diabetic kidney disease. *Cell Death Dis*. 2021;12(1):32. doi:10.1038/s41419-020-03312-0
10. Fu D, Senouthai S, Wang J, You Y. FKN facilitates HK-2 cell EMT and tubulointerstitial lesions via the Wnt/β-catenin pathway in a murine model of lupus nephritis. *Front Immunol*. 2019;10:784. doi:10.3389/fimmu.2019.00784
11. Imai T, Yasuda N. Therapeutic intervention of inflammatory/immune diseases by inhibition of the fractalkine (CX3CL1)-CX3CR1 pathway. *Inflamm Regen*. 2016;36:9. doi:10.1186/s41232-016-0017-2
12. Shah R, Matthews GJ, Shah RY, et al. Serum fractalkine (CX3CL1) and cardiovascular outcomes and diabetes: findings from the Chronic Renal Insufficiency Cohort (CRIC) Study. *Am J Kidney Dis*. 2015;66(2):266–273. doi:10.1053/j.ajkd.2015.01.021
13. Song KH, Park J, Park JH, Natarajan R, Ha H. Fractalkine and its receptor mediate extracellular matrix accumulation in diabetic nephropathy in mice. *Diabetologia*. 2013;56(7):1661–1669. doi:10.1007/s00125-013-2907-z
14. Navarro-González JF, Mora-Fernández C, de Fuentes MM, García-Pérez J, Muros de Fuentes M, García-Pérez J. Inflammatory molecules and pathways in the pathogenesis of diabetic nephropathy. *Nat Rev Nephrol*. 2011;7(6):327–340. doi:10.1038/nrneph.2011.51
15. Kikuchi Y, Ikee R, Hemmi N, et al. Fractalkine and its receptor, CX3CR1, upregulation in streptozotocin-induced diabetic kidneys. *Nephron Exp Nephrol*. 2004;97(1):e17–e25. doi:10.1159/000077594
16. Kikuchi Y, Imakiire T, Hyodo T, et al. Advanced glycation end-product induces fractalkine gene upregulation in normal rat glomeruli. *Nephrol Dial Transplant*. 2005;20(12):2690–2696. doi:10.1093/ndt/gfi232
17. Donadelli R, Zanchi C, Morigi M, et al. Protein overload induces fractalkine upregulation in proximal tubular cells through nuclear factor kappaB- and p38 mitogen-activated protein kinase-dependent pathways. *J Am Soc Nephrol*. 2003;14(10):2436–2446. doi:10.1097/01.ASN.0000089564.55411.7F
18. Adekoya TO, Richardson RM. Cytokines and chemokines as mediators of prostate cancer metastasis. *Int J Mol Sci*. 2020;21:12. doi:10.3390/ijms21124449
19. Miyazono K, Ehata S, Koinuma D. Tumor-promoting functions of transforming growth factor-β in progression of cancer. *Ups J Med Sci*. 2012;117(2):143–152. doi:10.3109/03009734.2011.638729
20. Dongre A, Weinberg RA. New insights into the mechanisms of epithelial-mesenchymal transition and implications for cancer. *Nat Rev Mol Cell Biol*. 2019;20(2):69–84. doi:10.1038/s41580-018-0080-4
21. Zhang L, Shen ZY, Wang K, et al. C-reactive protein exacerbates epithelial-mesenchymal transition through Wnt/β-catenin and ERK signaling in streptozocin-induced diabetic nephropathy. *FASEB J*. 2019;33(5):6551–6563. doi:10.1096/fj.201801865RR
22. Guo H, Cao A, Chu S, et al. Astragaloside IV attenuates podocyte apoptosis mediated by endoplasmic reticulum stress through upregulating sarco/endoplasmic reticulum Ca(2+)-ATPase 2 expression in diabetic nephropathy. *Front Pharmacol*. 2016;7:500. doi:10.3389/fphar.2016.00500
23. Cao Y, Zhang L, Wang Y, Fan Q, Cong Y. Astragaloside IV attenuates renal fibrosis through repressing epithelial-to-mesenchymal transition by inhibiting microRNA-192 expression: in vivo and in vitro studies. *Am J Transl Res*. 2019;11(8):5029–5038.
24. Zhang Y, Tao C, Xuan C, Jiang J, Cao W. Transcriptomic analysis reveals the protection of astragaloside IV against diabetic nephropathy by modulating inflammation. *Oxid Med Cell Longev*. 2020;2020:9542165. doi:10.1155/2020/9542165
25. Fan Y, Fan H, Zhu B, Zhou Y, Liu Q, Astragaloside LP. IV protects against diabetic nephropathy via activating eNOS in streptozotocin diabetes-induced rats. *BMC Complement Altern Med*. 2019;19(1):355. doi:10.1186/s12906-019-2728-9
26. Chen J, Chen Y, Luo Y, Gui D, Huang J, He D. Astragaloside IV ameliorates diabetic nephropathy involving protection of podocytes in streptozotocin induced diabetic rats. *Eur J Pharmacol*. 2014;736:86–94. doi:10.1016/j.ejphar.2014.04.037
27. Zhou XT, Zou JJ, Ao C, Gong DY, Chen X, Ma YR. Renal protective effects of astragaloside IV, in diabetes mellitus kidney damage animal models: a systematic review, meta-analysis. *Pharmacol Res*. 2020;160:105192. doi:10.1016/j.phrs.2020.105192
28. Wang H, Zhuang Z, Huang YY, et al. Protective effect and possible mechanisms of astragaloside IV in animal models of diabetic nephropathy: a preclinical systematic review and meta-analysis. *Front Pharmacol*. 2020;11:988. doi:10.3389/fphar.2020.00988
29. Feng H, Zhu X, Tang Y, Fu S, Kong B, Liu X. Astragaloside IV ameliorates diabetic nephropathy in db/db mice by inhibiting NLRP3 inflammasome-mediated inflammation. *Int J Mol Med*. 2021;48(2). doi:10.3892/ijmm.2021.4996
30. Su Y, Chen Q, Ma K, et al. Astragaloside IV inhibits palmitate-mediated oxidative stress and fibrosis in human glomerular mesangial cells via downregulation of CD36 expression. *Pharmacol Rep*. 2019;71(2):319–329. doi:10.1016/j.pharep.2018.12.008
31. Wang X, Gao Y, Tian N, et al. Astragaloside IV inhibits glucose-induced epithelial-mesenchymal transition of podocytes through autophagy enhancement via the SIRT-NF-κB p65 axis. *Sci Rep*. 2019;9(1):323. doi:10.1038/s41598-018-36911-1
32. Du L, Qian X, Li Y, et al. Sirt1 inhibits renal tubular cell epithelial-mesenchymal transition through YY1 deacetylation in diabetic nephropathy. *Acta Pharmacol Sin*. 2021;42(2):242–251. doi:10.1038/s41401-020-0450-2
33. Zhu J, Wen K. Astragaloside IV inhibits TGF-β1-induced epithelial-mesenchymal transition through inhibition of the PI3K/Akt/NF-κB pathway in gastric cancer cells. *Phytother Res*. 2018;32(7):1289–1296. doi:10.1002/ptr.6057
34. Wang YN, Zhao SL, Su YY, et al. Astragaloside IV attenuates high glucose-induced EMT by inhibiting the TGF-β/Smad pathway in renal proximal tubular epithelial cells. *Biosci Rep*. 2020;40(6). doi:10.1042/BSR20190987
35. He T, Xiong J, Nie L, et al. Resveratrol inhibits renal interstitial fibrosis in diabetic nephropathy by regulating AMPK/NOX4/ROS pathway. *J Mol Med*. 2016;94(12):1359–1371. doi:10.1007/s00109-016-1451-y
36. Dong Z, Sun Y, Wei G, Li S, Zhao Z. A nucleoside/nucleobase-rich extract from cordyceps sinensis inhibits the epithelial-mesenchymal transition and protects against renal fibrosis in diabetic nephropathy. *Molecules*. 2019;24:22. doi:10.3390/molecules24224119
37. Lamouille S, Xu J, Derynck R. Molecular mechanisms of epithelial-mesenchymal transition. *Nat Rev Mol Cell Biol*. 2014;15(3):178–196. doi:10.1038/nrm3758
38. Makrodouli E, Oikonomou E, Koc M, et al. BRAF and RAS oncogenes regulate Rho GTPase pathways to mediate migration and invasion properties in human colon cancer cells: a comparative study. *Mol Cancer*. 2011;10:118. doi:10.1186/1476-4598-10-118

39. Cox SN, Sallustio F, Serino G, et al. Activated innate immunity and the involvement of CX3CR1-fractalkine in promoting hematuria in patients with IgA nephropathy. *Kidney Int*. 2012;82(5):548–560. doi:10.1038/ki.2012.147
40. Shah R, Hinkle CC, Ferguson JF, et al. Fractalkine is a novel human adipochemokine associated with type 2 diabetes. *Diabetes*. 2011;60(5):1512–1518. doi:10.2337/db10-0956
41. Hou SM, Hou CH, Liu JF. CX3CL1 promotes MMP-3 production via the CX3CR1, c-Raf, MEK, ERK, and NF-κB signaling pathway in osteoarthritis synovial fibroblasts. *Arthritis Res Ther*. 2017;19(1):282. doi:10.1186/s13075-017-1487-6
42. Lee SJ, Namkoong S, Kim YM, et al. Fractalkine stimulates angiogenesis by activating the Raf-1/MEK/ERK- and PI3K/Akt/eNOS-dependent signal pathways. *Am J Physiol Heart Circ Physiol*. 2006;291(6):H2836–H2846. doi:10.1152/ajpheart.00113.2006